NASA TECHNICAL NOTE

NASA TN D-4440

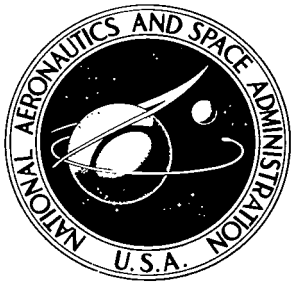

EXPERIMENTS ON STABILITY OF HERRINGBONE-GROOVED GAS-LUBRICATED JOURNAL BEARINGS TO HIGH COMPRESSIBILITY NUMBERS

by Robert E. Cunningham, David P. Fleming, and William J. Anderson

Lewis Research Center
Cleveland, Ohio

NATIONAL AERONAUTICS AND SPACE ADMINISTRATION • WASHINGTON, D. C. • APRIL 1968

NASA TN D-4440

EXPERIMENTS ON STABILITY OF HERRINGBONE-GROOVED GAS-LUBRICATED JOURNAL BEARINGS TO HIGH COMPRESSIBILITY NUMBERS

By Robert E. Cunningham, David P. Fleming, and William J. Anderson

Lewis Research Center
Cleveland, Ohio

NATIONAL AERONAUTICS AND SPACE ADMINISTRATION

For sale by the Clearinghouse for Federal Scientific and Technical Information
Springfield, Virginia 22151 – CFSTI price $3.00

EXPERIMENTS ON STABILITY OF HERRINGBONE-GROOVED GAS-LUBRICATED JOURNAL BEARINGS TO HIGH COMPRESSIBILITY NUMBERS

by Robert E. Cunningham, David P. Fleming, and William J. Anderson

Lewis Research Center

SUMMARY

Experiments were conducted with six rotors, $1\frac{1}{2}$ inches (3.8 cm) in diameter by $12\frac{1}{4}$ inches (31.1 cm) long and equipped with two herringbone-grooved journals. These rotors were operated in plain cylindrical sleeves to high compressibility numbers with ambient air as a lubricant. Vertical orientation of the rotors without any applied radial load presented a test condition most conducive to exciting half-frequency whirl (HFW). These experiments showed that HFW threshold speeds are very much dependent on radial clearance. Five rotors running at clearances from 370 to 500 microinches (9.4 to 12.7 μm) did not whirl up to the limiting speed of the air turbine drive. When the same rotors were operated at clearances ranging from 550 to 710 microinches (14 to 18 μm). HFW was experienced at fairly low speed ranges of from 14 750 to 27 900 rpm.

Limited test results comparing a fully grooved with a partially grooved rotor showed the fully grooved rotor to be stable up to 60 830 rpm. The partially grooved rotor having the same operating parameters except for groove length exhibited HFW at 27 900 rpm.

Agreement between experimental and theoretical results are generally quite good. Based on these results the theory tends to be somewhat conservative in defining zones of unstable operation.

Experiments have shown that it is possible to pass completely through a region of HFW instability without experiencing an excessive growth in the rotor amplitude and, at some higher speed, to revert back to stable operation. This is only true if the dimensionless mass number is not too large.

INTRODUCTION

Space turbomachinery of the type used in a closed loop, Brayton gas cycle must be compact and light weight. If the cycle gas is used as a lubricant, these machines are

more compact and lighter than machines using oils as lubricants. Components like oil sumps, contact seals, and oil scavenging and separating systems normally required with conventionally lubricated bearings are eliminated (ref. 1). A reduction in parasitic losses is an additional advantage gained by eliminating these auxiliary components.

A closed-loop cycle is one in which an inert gas is continuously recirculated. If the system is to operate reliably for many thousands of hours, this cycle gas must remain clean. Gas bearings are well suited to this application. Their use precludes the possibility of working fluid contamination because there is no direct contact of shaft and bearing during normal operation (ref. 2).

Bearing stability is of utmost importance and must be given careful consideration in the overall design. The shafts of any rotating machine are subject to certain types of vibratory motions. One type that is common to all rotating machines is a synchronous vibration produced by unbalanced forces in the rotor. The rotor tends to whirl in an orbit about the center of the bearing and its frequency is equal to the rotational speed of the rotor. The lubricating films, whether they be oil or gas, act like springs; consequently, the rotor bearing system has fundamental frequencies. When the orbiting frequency becomes equal to a system frequency, the amplitude of motion can become quite large, depending on the damping forces in the film. This frequency is referred to as a system critical speed. Most small turbomachines are designed to operate above the critical speed and therefore must pass through it. By precision balancing of the rotating parts, the amplitude of vibration at a critical speed can be kept quite small. Passing through the critical speed rapidly, therefore, presents no serious problem.

Lightly loaded rotors running in self-acting fluid film bearings are susceptible to another type of vibration not so easily delt with. This instability is a self-excited vibration produced by unbalanced pressure forces in the lubricating film. Lightly loaded rotors operate with high attitude angles and small eccentricity ratios. Under these conditions, the tangential component of the pressure force is quite large. The resulting moment drives the rotor in an orbital path about the bearing center and in the direction of rotation. The frequency of this orbital motion is approximately one-half that of the rotor speed and, hence, has been given the name half-frequency whirl (HFW) (ref. 3).

Sufficient viscous damping is usually present in oil lubricated journal bearings to limit the size of the whirl amplitude. However, when the lubricant is a gas having low damping characteristics, rotor whirl persists and grows in size with increasing rotor speeds. If the amplitude becomes large enough, the shaft and bearing touch, and severe damage to shaft and bearing is likely to result.

Numerous papers have been written that attempt to predict theoretically the onset of half-frequency whirl (refs. 4 to 6). A difficult problem arises, however, in attempting to solve the time dependent Reynolds equation for compressible flow. The assumptions, necessary in even the most complex of mathematical models, limit the accuracy

of results. It is essential, therefore, to supplement the theoretical analysis with experimentation.

A number of self-acting bearing designs have evolved that have somewhat stable operating characteristics. These designs shape the bearing surface to create artificial fluid film wedges in the absence of any applied radial load. Radial restoring forces are generated which tend to keep the journal from whirling. Listed in the order of least to most stable operation are (1) elliptical bearings, (2) three and four lobe bearings, and (3) three and four sector tilting pad bearings. References 7 and 8 give a more detailed analysis of their operating characteristics. All these designs achieve a certain degree of stability, but at the expense of load capacity. An additional disadvantage of the tilting pad bearing is its complexity. Each shoe is independently mounted on a pivot. This allows each shoe to pivot and, thus, conform to the rotor attitude. Some additional method of adjustment is usually required on at least one of the shoes to obtain alinement at assembly.

The helical grooved or the herringbone-grooved bearing shows the most promise of stable operation with no sacrifice in load capacity (refs. 9 and 10). Shallow grooves formed in a herringbone pattern act like a viscous pump when the shaft turns (see fig. 1). Air is pumped from the bearing ends toward the middle. The pressure distribution that results is similar to that obtained in a hydrostatic bearing. Attitude angles in herringbone-grooves and hydrostatic bearings tend to be small and radial restoring forces high. The difference, however, is that the pressure in a herringbone bearing increases with increasing speed.

The objectives of this study were (1) to investigate experimentally the stability characteristics of the herringbone-grooved gas-journal bearing to high compressibility numbers and (2) to compare the test results with existing stability theory (ref. 11). The following characteristics and their effects on threshold of HFW were examined: (1) Helix angle, (2) number of grooves, (3) partial and full grooving, and (4) clearance.

Six rotors, $1\frac{1}{2}$ inches (3.8 cm) in diameter by $12\frac{1}{4}$ inches (31.1 cm) long equipped with two herringbone-grooved journals having varying geometries were tested to speeds of 60 830 rpm. The rotors were mounted in two cylindrical bronze sleeves and operated in a vertical position to negate gravitational forces. The dynamic attitude of the rotors in the bearings was continously monitored and whirl onset speeds recorded. Different sets of bronze sleeves were used to determine the effects of clearances on whirl onset speeds.

SYMBOLS

a_g width of helical groove, in.; cm

a_r width of helical land, in.; cm

C	bearing radial clearance, in.; cm
D	rotor diameter, in.; cm
e	rotor eccentricity, in.; cm
F_r	radial bearing force
F_t	tangential force
H	ratio of groove clearance to ridge clearance, h_g/h_r
h_g	groove clearance, in.; cm
h_r	ridge clearance, in.; cm
L	bearing length, in.; cm
L_1	length of grooved portion of bearing, in.; cm
M	mass of rotor per bearing, (lb)(sec^2)/in.; (kg)(sec^2)/cm
$\overline{M}$	dimensionless mass parameter, $M P_a R/\mu^2 LD (C/R)^5$
N	shaft speed, rpm
N_s	half-frequency whirl onset speed, rpm
n	number of grooves
P_a	atmospheric pressure, psia; N/m^2
R	rotor radius, in.; cm
W	total weight of rotor, lb; kg
Y	ratio of grooved portion of bearing to total bearing length, L_1/L
α	ratio of groove width to total width, groove plus land, $a_g/(a_g + a_r)$
β	helix angle, deg
ϵ	journal eccentricity ratio, e/C
ω	angular rotor speed, rad/sec
δ	groove depth, in.; cm
Λ	compressibility number, $\frac{6\mu\omega}{P_a}\left(\frac{R}{C}\right)^2$
μ	absolute viscosity, (lb)(sec)/in.^{2}; (kg)(sec)/cm^2

APPARATUS

The apparatus used in conducting these tests is shown schematically in figure 2. A

steel rotor, $1\frac{1}{2}$ inches (3.8 cm) in diameter and $12\frac{1}{4}$ inches (31.1 cm) long, is mounted vertically in two smooth cylindrical bronze sleeves. Two herringbone-grooved patterns in the rotor surface and centered in two bronze sleeves comprise the bearing assembly. Groove patterns extend beyond the end of the sleeves to ensure a supply of ambient air. The sleeves are $1\frac{1}{2}$ inches (3.8 cm) long. Axial centerline distance between the two sleeves is $6\frac{5}{8}$ inches (16.9 cm). An externally pressurized pocket thrust bearing supports the rotor at its lower end.

The rotors are driven by an impulse turbine assembly. It consists of ten 1/8-inch (0.32-cm) diameter nozzles and six equally spaced turbine buckets machined into the rotor at its upper end. A solid-state electronic controller was used to regulate the turbine air supply and thus accurately maintain a preset rotor speed. A magnetic pick-up in close proximity to the turbine buckets monitored rotor speed and was the sensing element in the speed control system.

Instrumentation

Two orthogonally oriented capacitance distance probes were located in the same radial plane and outboard of each bearing. These probes provided a noncontacting method of detecting radial displacement of the rotor. A fifth capacitance probe, mounted flush with the thrust bearing surface, was used to monitor thrust bearing clearance.

Each of these probes, with its own capacitance distance meter, cables, and filters (see fig. 3), were calibrated before assembly into the test apparatus. Calibration of these capacitance probes was done using accurate gage blocks. Because the probes face a curved surface, the observed readings had to be corrected. This was done using a table of values supplied by the probe manufacturer. An X-Y curve tracing cathod ray oscilloscope (CRO) was used to display the signals generated by the probes of both upper and lower bearings. Either an orbital motion trace or displacement as a function of time trace could be displayed.

TEST ROTORS

Two of the experimental herringbone-grooved rotors used in this stability investigation are shown in the photographs of figure 1. Six rotors, each with a different groove geometry, were evaluated and are listed in table I. The rotors were made of AMS-5643, precipitation hardening stainless steel. Hardness varied from 42 to 45 on the Rockwell C scale.

Measurements of concentricity and roundness made with two different types of geometry gages showed good agreement. Concentricity measurements made at three

places along the rotor length averaged 20 microinches (0.5 μm) total indicator runout (TIR), the maximum reading being 35 microinches (0.9 μm) TIR. The rotors were machined round within 20 microinches (0.5 μm) TIR (average reading), the maximum being 30 microinches (0.8 μm) TIR. Readings of diametral taper every 3 inches (7.6 cm) of rotor length averaged 30 microinches (0.8 μm). The maximum was 70 microinches (1.8 μm). Maximum diameters measured were at the rotor midspans, indicating a slight barrel shape to the rotors. Diameter measurements were made at four different places along the rotor length. An electronic dial indicator, accurate to 10 microinches (0.25 μm), was used to make these measurements. Surface finishes were from 3 to 4 microinches (0.08 to 0.1 μm) rms.

The aluminum bronze sleeves into which the herringbone-grooved rotors were assembled were in-line bored and lapped. The inside diameters were measured at several places along the sleeve using an air gage with an accuracy of 10 microinches (0.25 μm). Roundness, concentricity, and taper of sleeves were as good or better than those of the rotors. A typical surface profile trace made on two of the subsurface herringbone-grooves are shown in figure 4. The average depths of grooves for each rotor are listed in table I.

Procedure

Prior to assembly, the surface of each rotor was thoroughly cleansed with alcohol. After the rotor had been assembled, clearances in two orthogonal planes, for both upper and lower bearings, were measured using the calibrated capacitance probes. This was also done after each test. These clearances were compared closely with previously measured bearing bore and rotor diameter measurements.

Each rotor was accelerated to speed and its synchronous whirl orbit noted. If the amplitude of unbalance was too large for any given rotor, the rotor was balanced with the aid of a reference marker (flat spot on rotor directly under each capacitance probe). This reference marker occurs on the CRO amplitude-time trace once per revolution. The plane of maximum rotor excursion relative to the reference marker is easily determined.

After balancing, each rotor was then accelerated to speed, and the threshold of HFW was noted, if and when it occurred. If HFW occurred, the speed was slowly increased beyond the threshold speed. The test was stopped if the whirl amplitude grew rapidly. If the amplitude remained small, the speed was increased to the limiting speed of the air turbine drive.

RESULTS AND DISCUSSION

Experimental results obtained on six rotors with different groove geometries are shown in tables I and and in figures 5 to 10. The rotors were operated in air at standard conditions and up to a maximum bearing compressibility number of 45.

The decided influence of radial clearance on stability is readily apparent when comparing results of table I. For a radial clearance range of 550 to 710 microinches (14 to 18 μm), all five partially grooved rotors exhibited half-frequency whirl. Whirl onset speed was the lowest for rotor A-5, which had the largest clearance of 710 microinches (18 μm). The highest HFW threshold speed occurred with rotor A-1, which had the smallest assembled radial clearance of 550 microinches (14 μm). When the same five rotors were operated at clearances ranging from 370 to 500 microinches (9.4 to 12.7 μm) (see table I), none of the rotors whirled up to the maximum speed of 59 000 rpm. Helix angles and number of grooves were varied. Groove-width to land-width ratios α and groove length to overall length ratio Y were held constant for rotors A-1 to A-5. Rotor diameter, length, weight, and bearing span were also held constant.

Figure 5 shows the amplitude-time trace of rotor A-1 running in the high-clearance sleeves. HFW threshold speed was 27 900 rpm. At 30 000 rpm, the amplitude was 275 microinches (7 μm). At 35 000 rpm, the amplitude had increased to 413 microinches (10.5 μm). A further increase in speed showed no additional growth of the whirl orbit. At a speed of 48 000 rpm, the shaft motion became synchronous having an amplitude of approximately 75 microinches (1.9 μm). This low-amplitude synchronous whirl was observed up to the maximum speed of 56 500 rpm, which was the upper limiting speed imposed by the air turbine drive.

Figure 6 shows the stable operation of rotor A-1 in low-clearance sleeves up to a maximum turbine drive speed of 55 000 rpm.

Theory predicts that a fully grooved herringbone bearing, of the type depicted in figure 1(b), should be more stable than a partially grooved bearing, shown in figure 1(a). To verify this, a fully grooved rotor designated B-1 was made which was to be identical to A-1 except for length of grooves. The vendor, however, experienced difficulty in fabricating the groove pattern in B-1; consequently, the grooves are considerably more shallow than in A-1 (330 rather than 580 microinches (8.4 rather than 14.7 μm)). In addition, B-1 was slightly larger in diameter, resulting in a clearance of 530 microinches (13.5 μm) for B-1, compared with 550 microinches (14 μm) for A-1. The slightly smaller clearance would marginally increase stability; however, theory predicts that the shallow grooves on B-1 should make that rotor considerably less stable than an equivalent rotor with the groove depth of A-1. Despite this, rotor B-1 was run to a speed of 60 830 rpm without any HFW being observed. It is concluded, therefore, that,

in addition to clearance, the length of grooves is an important factor in the stability of a bearing.

Figures 7 to 10 show a comparison of the experimental results with the theory. Shown in these stability plots is dimensionless rotor mass parameter as a function of dimensionless compressibility number. These curves are based on the work described in reference 11 and are also briefly outlined in the appendix of this report.

Neither of the two experimental curves in figure 7 intersect the theoretical HFW region. Rotor A-1, at a zero-speed clearance of 550 microinches (14 μm), did, however, actually pass through the HFW region. The HFW threshold speed observed was 27 900 rpm, corresponding to a compressibility number of 6.4. Return to stable operation occurred at a speed of 49 000 rpm, corresponding to a compressibility number of 13. The lower experimental curve for rotor A-1 at a zero speed clearance of 370 microinches (9.4 μm) falls far below the lowest portion of the HFW zone. The downward slope of the experimental curves is due to a decreasing clearance caused by centrifugal growth of the rotor. The amount of growth due to centrifugal effects was calculated.

Agreement between theory and experiment is generally good as shown by test results in the composite plot of figure 8 for rotors A-1 to A-5 for high clearance values. Data are included in figure 8 for four rotors run in a third set of bronze sleeves having clearances larger than those listed in table I. As would be expected, the HFW occurred at relatively low speeds under these conditions. It should be pointed out however, that some heating of the rotor and housing parts was observed during the test runs. Dimensional changes of the bronze sleeves and rotor could have resulted in larger clearances than those measured at the start of the tests. This would tend to raise the data points and result in better agreement. However, clearance measurements made at the end of a test did not show any definite pattern of clearance change.

Entry into the theoretical HFW region at high dimensionless mass numbers $\overline{M}$ not only occurs at a low threshold speed but, in addition, produces a high-amplitude whirl motion. This is shown by experimental results obtained for rotors A-2 and A-3 (fig. 9) and A-4 and A-5 (fig. 10) at high clearances. It was not possible to increase the speed much beyond the HFW threshold because of the rapid growth in the whirl orbit for small increases in speed. This was not the case with rotor A-1 (fig. 7) in high clearance sleeves. Here, it was possible to pass completely through the HFW region without experiencing an excessive whirl amplitude because of lower values of $\overline{M}$.

SUMMARY OF RESULTS

The results listed below were obtained with six $1\frac{1}{2}$-inch (3.8 cm) diameter by $12\frac{1}{4}$- inch (31.1 cm) long rotors operating in ambient air to a maximum compressbility

number of 45. The rotors containing herringbone-groove patterns at two locations were operated vertically in two cylindrical bronze sleeves. No external load was applied to the bearings.

1. Test results in low- and high-clearance sleeves indicate that half-frequency whirl (HFW) is most affected by the radial clearance. The five partially grooved rotors ran stably to maximum speeds of 55 000 and 59 000 rpm when clearances ranged from 370 to 500 microinches (9.4 to 12.7 μm). When clearances were increased from 550 to 710 microinches (14 to 18 μm), all five rotors experiences HFW.

2. Limited test results with two rotors with identical groove geometry, except for groove length, and comparable clearances indicate that a fully grooved bearing is more stable than a partially grooved one. Partially grooved rotor A-1 exhibated HFW at a speed of 27 900 rpm, although the fully grooved rotor B-1 ran to a maximum speed of 60 830 rpm without experiencing HFW.

3. Reasonably fair agreement between the experimental results and existing stability criteria was obtained. The stability analysis appears to be conservative in predicting ranges of unstable operation.

4. It was shown experimentally that a region of unstable operation (HFW) can be passed through without experiencing a sizable growth in the orbital amplitude, if the rotor mass parameter is kept small.

5. Within the range of helix angles and number of grooves investigated, no significant difference in stability was observed.

Lewis Research Center,
National Aeronautics and Space Administration,
Cleveland, Ohio, November 29, 1967,
129-03-13-05-22.

APPENDIX

STABILITY CRITERION FOR JOURNAL BEARING

Stability limits for unloaded journal bearings may be found from the solutions for steady whirling of the bearing or journal (ref. 11). According to the theory, a bearing is neutrally stable when the tangential force F_t is zero and the centrifugal force due to whirling $Me\omega_3^2$ is exactly balanced by the radial bearing force F_R (fig. 11). The analysis used to find steady-state operating characteristics (ref. 9) includes a term for steady whirling. Thus, only the whirl frequencies ω_3, for which the tangential force is zero, must be found. The whirling mass whose centrifugal force is just balanced by the radial bearing force is the critical mass M_C for this condition. In dimensionless form

$$\frac{M_C}{LD}\left(\frac{C}{R}\right)^5 \frac{RP_a}{\mu^2} = \frac{36}{\Lambda^2} \frac{F_R}{\epsilon P_a LD} \left(\frac{\omega}{\omega_3}\right)^2$$

The bearing will be stable for values of M incrementally less than M_C, if the derivative of tangential force with whirl frequency $\partial F_t/\partial\omega_3$ is negative; the bearing will become unstable for M incrementally greater than M_C. The reverse holds if $\partial F_t/\partial\omega_3 > 0$.

REFERENCES

1. Stewart, Warner L.; Anderson, William J.; Bernatowicz, Daniel T.; Guentert, Donald D.; Packe, Donald E.; and Rohlik, Harold E.: Brayton Cycle Technology. Space Power Systems Advanced Technology Conference. NASA SP 131, 1966, pp. 95-145.

2. Curwen, P. W.; Frost, A.; and Arwas, E. B.: Gas Bearing Systems for NASA Solar Brayton Cycle Axial Flow Turbocompressor and Turboalternator. Paper Presented at ASME Spring Lubrication Symposium New York, June 9, 1965.

3. Sternlicht, B.; Poritsky, H.; and Arwas, E.: Dynamic Stability Aspects of Cylindrical Journal Bearings Using Compressible and Incompressible Fluids. First International Symposium on Gas Lubricated Bearings, Office of Naval Research, 1959, pp. 119-160.

4. Sternlicht, B.; and Winn, L. W.: Geometry Effects on the Thrushold of Half-Frequency Whirl in Self-Acting, Gas-Lubricated Journal Bearings. J. Basic Eng., vol. 86, no. 2, June 1964, pp. 313-320.

5. Constantinescu, V. N.: On Hydrodynamic Instability of Gas-Lubricated Journal Bearings. J. Basic Eng., vol. 87, no. 3, Sept. 1965, pp. 579-588.

6. Pan, C. H. T.; and Sternlicht, B.: Comparison Between Theories and Experiments for the Threshold of Instability of Rigid Rotor in Self-Acting, Plain-Cylindrical Journal Bearings. J. Basic Eng., vol. 86, no. 2, June 1964, pp. 321-327.

7. Pinkus, O.: Sleeve Bearing Design. Product Eng., vol. 26, no. 8, Aug. 1955, pp. 134-139.

8. Gunter, E. J., Jr.; Hinkle, J. G.; and Fuller, D. D.: The Effects of Speed, Load, and Film Thickness on the Performance of Gas-Lubricated, Tilting-Pad Journal Bearings. ASLE Trans., vol. 7, no. 4, Oct. 1964, pp. 353-365.

9. Vohr, J. H.; and Chow, C. Y.: Characteristics of Herringbone-Grooved, Gas-Lubricated Journal Bearings. J. Basic Eng., vol. 87, no. 3, Sept. 1965, pp. 568-578.

10. Malanoski, S. B.: Experiments on an Ultra-Stable Gas Journal Bearing. ASME Paper No. 66, LUB 6, or MTI No. 65, TR-37.

11. Pan, C. H. T.: Spectral Analysis of Gas Bearing Systems for Stability Studies. Rep. No. MTI-64-TR58, Mechanical Technology, Inc., Dec. 15, 1964. (Available from DDC as AD-610870.)

TABLE I. - TEST RESULTS OF HERRINGBONE-GROOVED ROTORS

[Groove-width to total-width ratio, 0.5; groove-length to total-bearing-length ratio, 0.6; total rotor weight, 6.06 lb (2.75 kg); rotor length, 12.25 in. (31.1 cm); bearing span, 6.64 in. (16.9 cm); nominal rotor diameter, 1.5 in. (3.8 cm); bearing length to diameter ratio, 1.0.]

Rotor number	Helix angle β, deg	Number of grooves n	Ratio of groove clearance to ridge clearance, H	Groove depth, (a)		Zero-speed radial clearance, (b)		HFW threshold speed N_s, rpm	Maximum rotor speed, rpm	Remarks
				μin.	μm	μin.	μm			
High clearances										
A-1	30	20	2.1	580	14.7	550	14.0	27 900	[c]56 500	Bounded whirl orbit, no HFW above 48 000 rpm
A-2	35	20	2.0	640	16.2	620	15.7	15 700	18 250	Unstable HFW orbit grows rapidly with increasing speed
A-3	35	23	1.9	540	13.7	600	15.2	22 300	24 130	↓
A-4	40	23	2.1	610	15.5	580	14.7	20 900	21 700	
A-5	40	28	2.0	710	18.0	710	18.0	14 750	16 000	
[d]B-1	30	20	1.6	330	8.4	530	13.5	------	[c]60 830	No HFW observed
Low clearances										
A-1	30	20	2.6	580	14.7	370	9.4	------	[c]55 000	Stable operation to maximum speed
A-2	35	20	2.4	640	16.2	470	11.9	------	[c]59 000	
A-3	35	23	2.5	540	13.7	350	8.9	------	[c]56 200	↓
A-4	40	23	2.6	610	15.5	390	9.9	------	[c]55 000	
A-5	40	28	2.4	710	18.0	500	12.7	------	[c]59 000	

[a]Depth measured with surface profile tracer (readings averaged).

[b]Assembled clearance measured at zero speed.

[c]Limiting speed with air turbine drive.

[d]Fully grooved, $Y = L_1/L = 1.0$.

C-67-1121

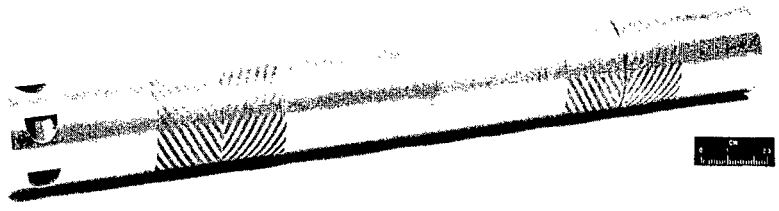

C-67-1153

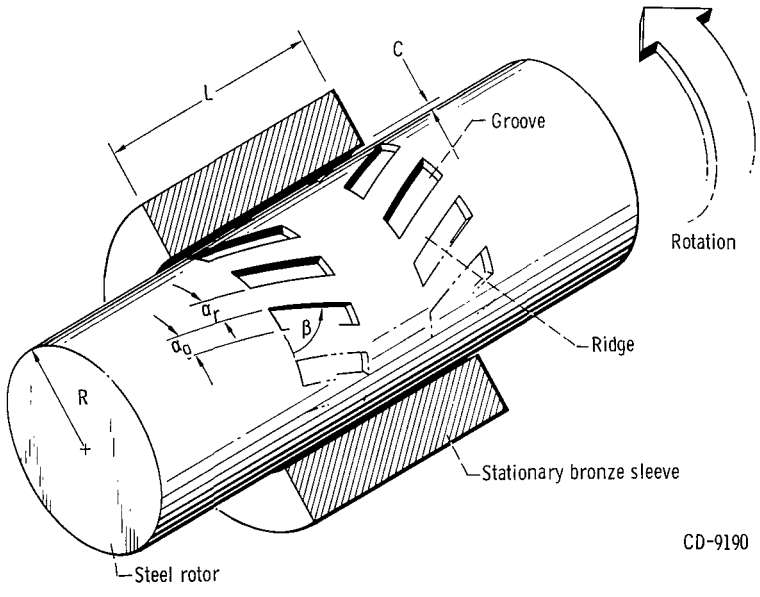

(a) Partially grooved rotors A-1 to A-5.

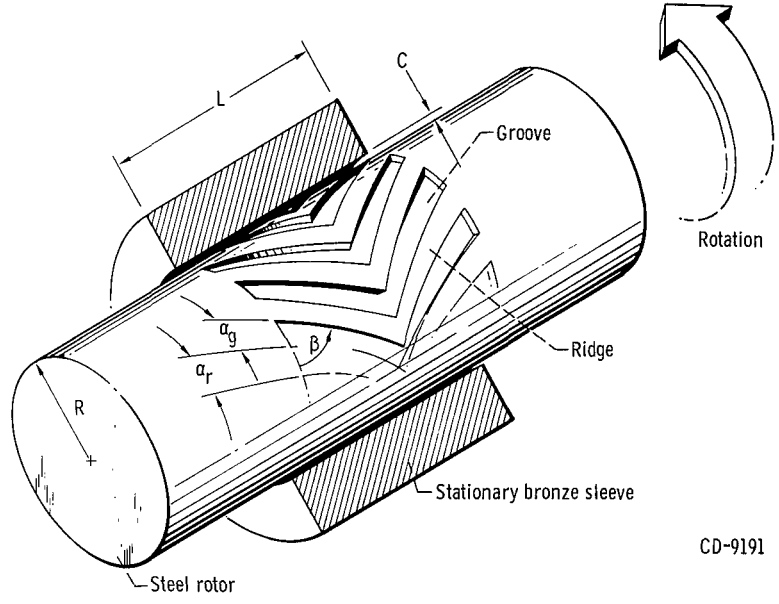

(b) Fully grooved rotor B-1.

Figure 1. - Herringbone-groove bearings.

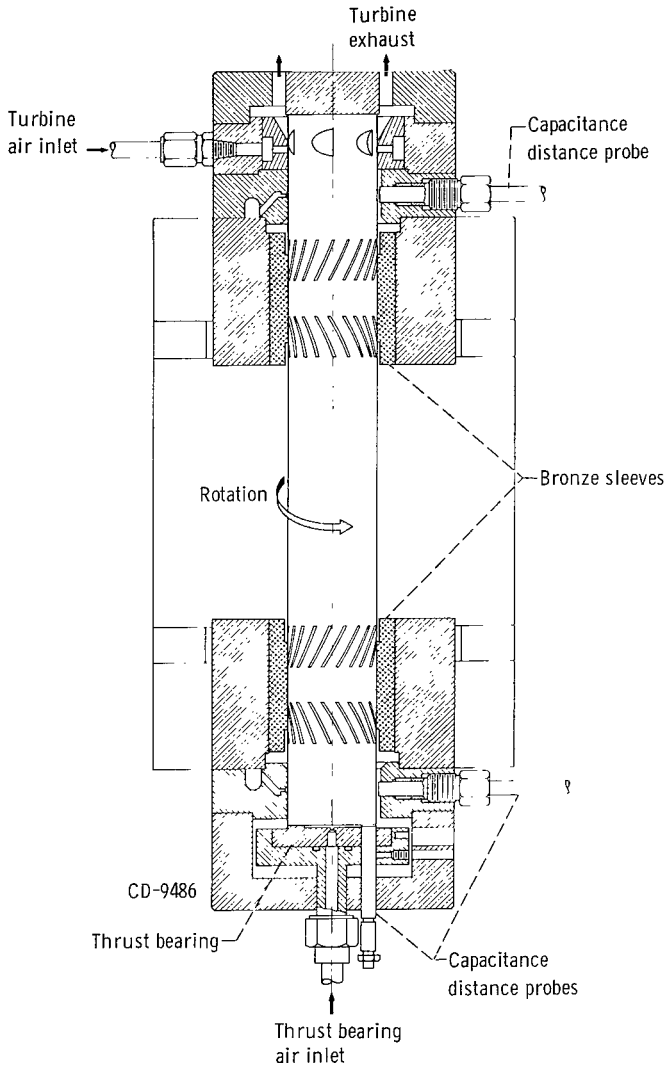

Figure 2. - Test apparatus.

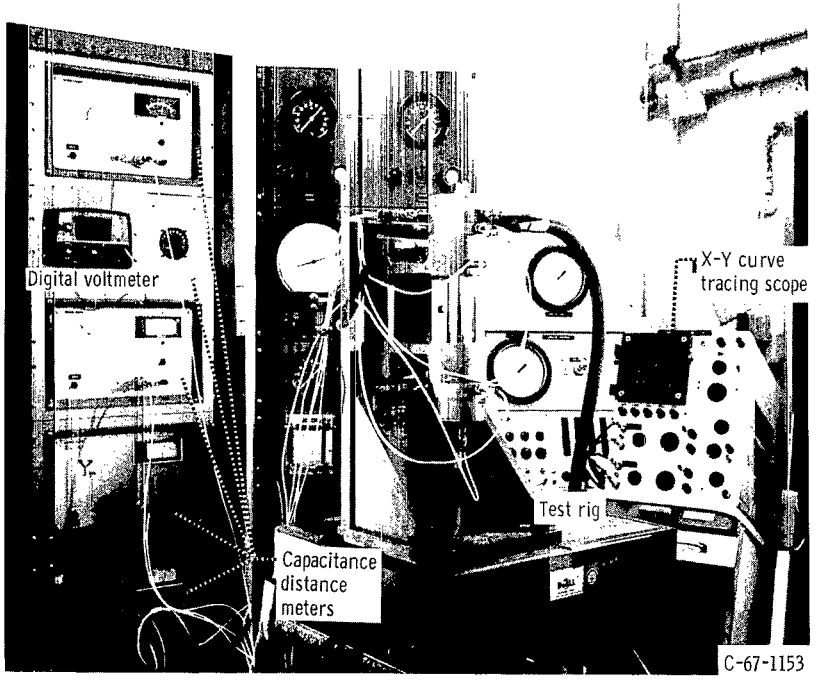

Figure 3. - Test apparatus in vertical position with readout instrumentation.

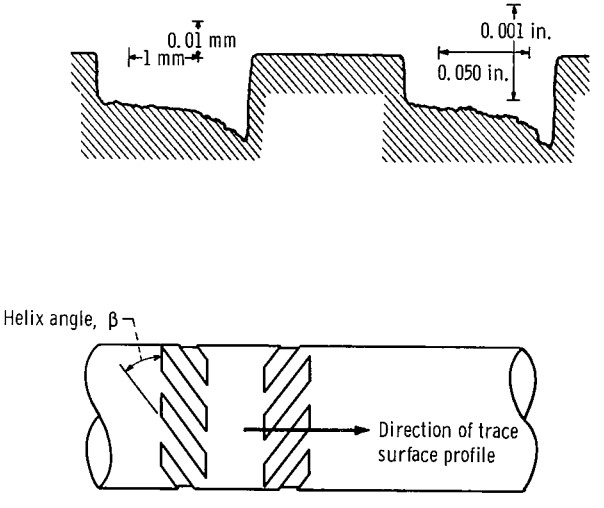

Figure 4. - Typical surface profile trace and representation of herringbone grooves on rotor.

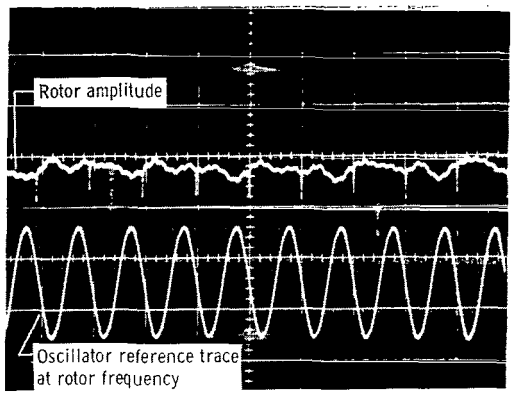

(a) Synchronous rotor motion at 12 000 rpm; amplitude, 4.5 microinches (0.11 μm).

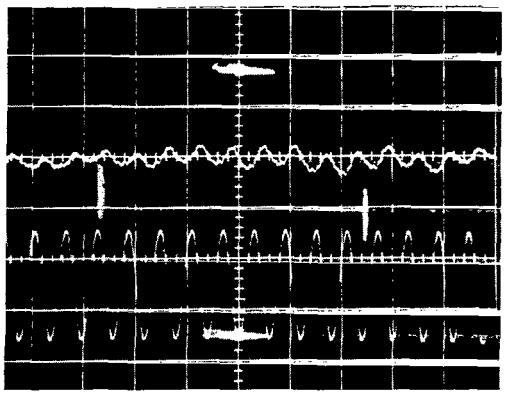

(b) Synchronous rotor motion at 20 000 rpm; amplitude, 6 microinches (0.15 μm).

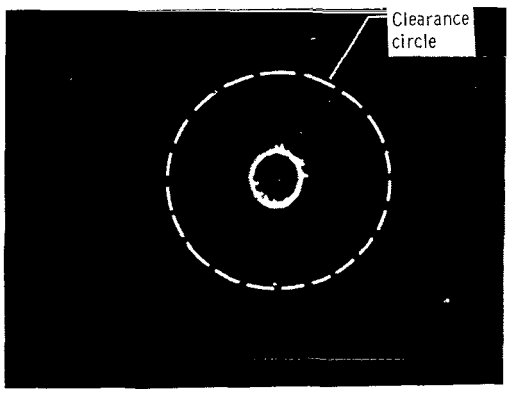

(c) X-Y trace of rotor motion in HFW. Rotor speed, 30 000 rpm; diameter of orbit, 275 microinches (6.8 μm).

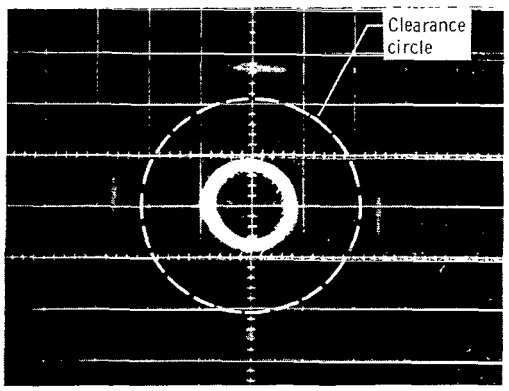

(d) X-Y trace of rotor motion in HFW. Rotor speed, 35 000 rpm; diameter of orbit, 413 microinches (10.5 μm).

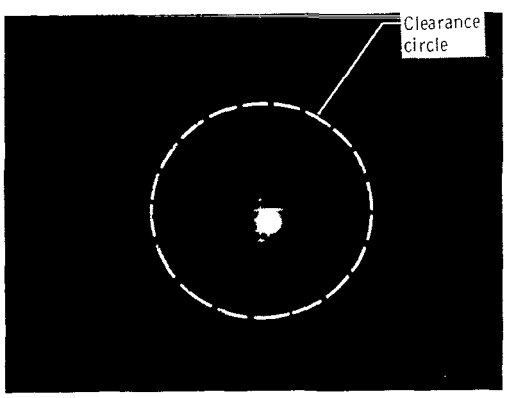

(e) X-Y trace of synchronous rotor motion at 50 000 rpm; amplitude, 75 microinches (1.9 μm).

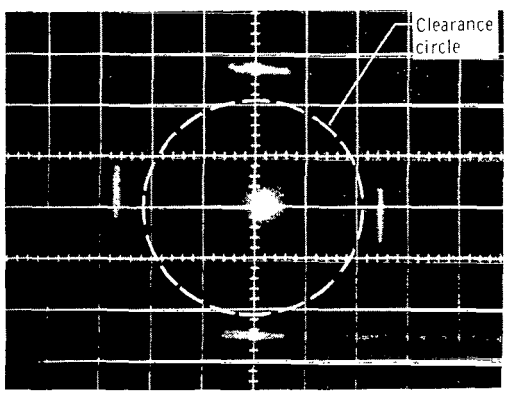

(f) X-Y trace of synchronous rotor motion at 55 230 rpm; amplitude, 75 microinches (1.9 μm).

Figure 5. - Motion of herringbone-grooved rotor A-1 in high-clearance bearing sleeves. Helix angle, 30°; number of grooves, 20; groove clearance to ridge clearance ratio, 2.1; groove length to total bearing length ratio, 0.6; groove width to total width ratio, 0.5; bearing radial clearance, 550 microinches (14 μm).

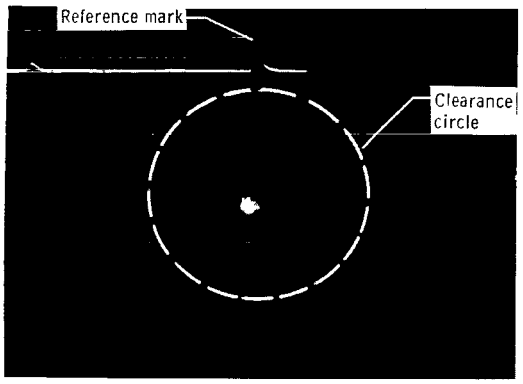

(a) Synchronous rotor motion at 11 000 rpm; negligible amplitude.

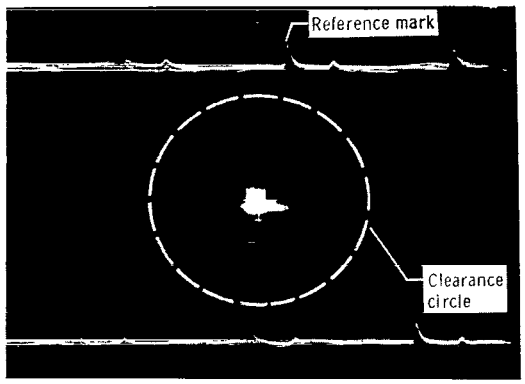

(b) Synchronous rotor motion at 20 000 rpm; negligible amplitude.

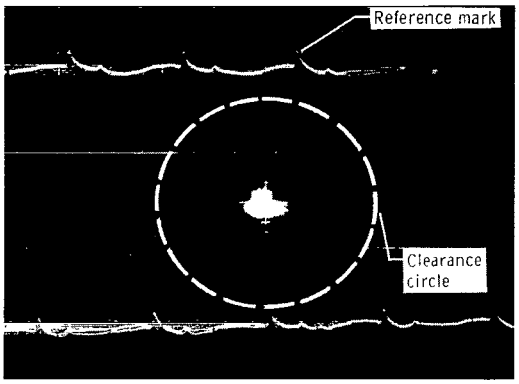

(c) Synchronous rotor motion at 30 000 rpm; amplitude, approximately 50 microinches (1.3 μm).

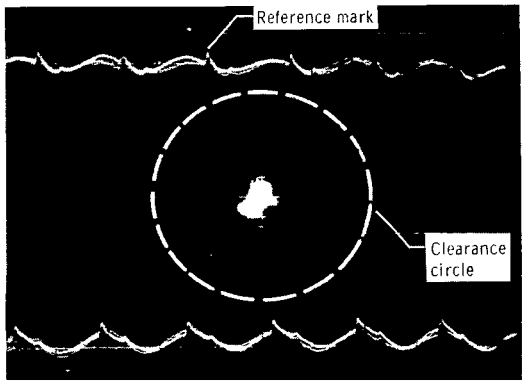

(d) Synchronous rotor motion at 40 000 rpm; amplitude, approximately 60 microinches (1.5 μm).

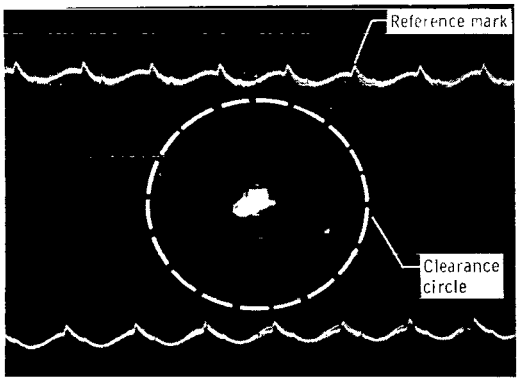

(e) Synchronous rotor motion at 50 000 rpm; amplitude, approximately 75 microinches (1.9 μm).

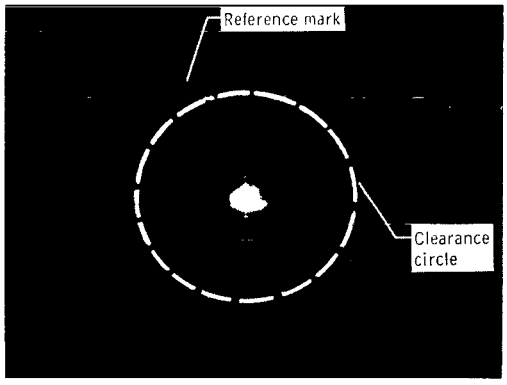

(f) Synchronous rotor motion at 55 000 rpm; amplitude, approximately 75 microinches (1.9 μm).

Figure 6. - X-Y and amplitude-time traces of herringbone-grooved rotor A-1 in low-clearance sleeves. Helix angle, 30°; number of grooves, 20; groove clearance to ridge clearance ratio, 2.6; groove length to total bearing length ratio, 0.6; groove width to total width ratio, 0.5; bearing radial clearance, at zero speed, 370 microinches (9.4 μm).

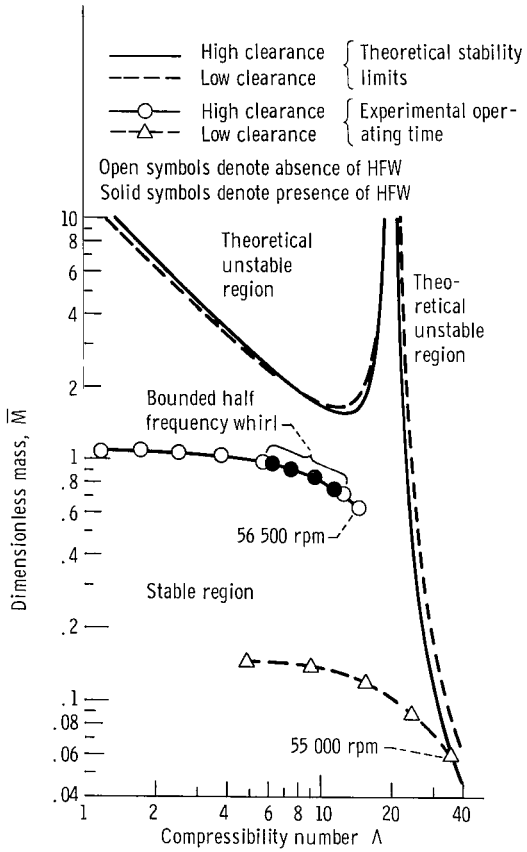

Figure 7. - Comparison of theoretical and experimental stability data for rotor A-1.

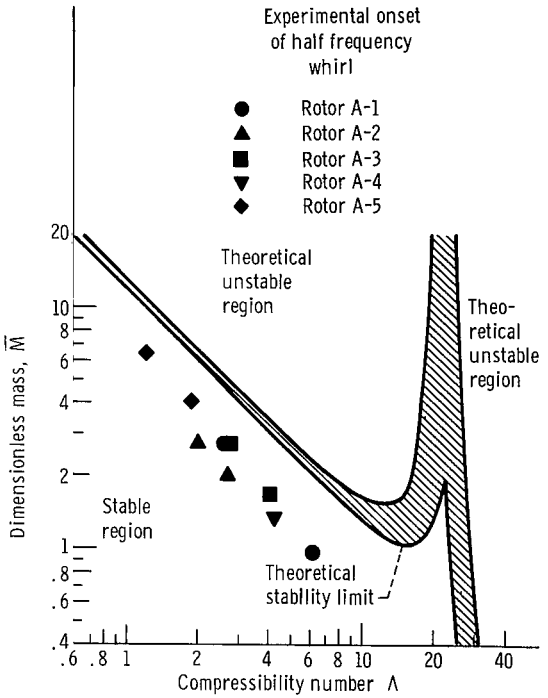

Figure 8. - Composite stability map for rotors A-1 through A-5 in high clearance bearings.

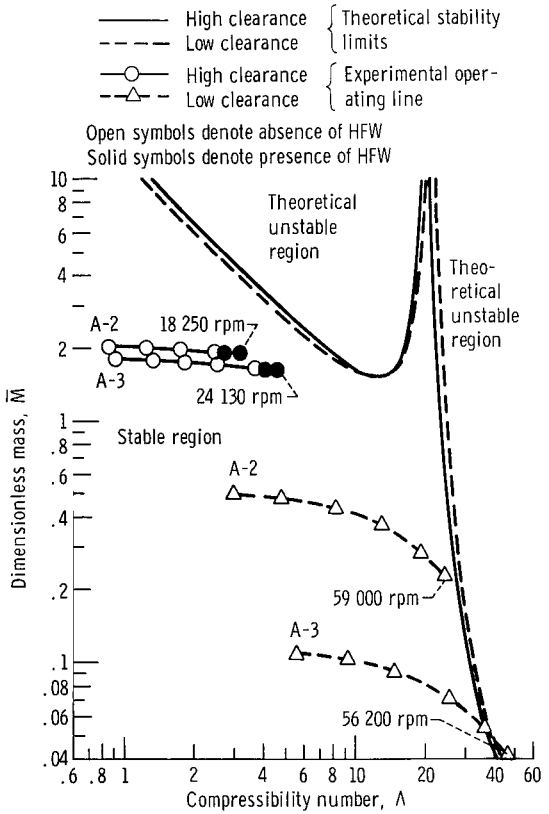

Figure 9. - Comparison of theoretical and experimental stability data for rotors A-2 and A-3.

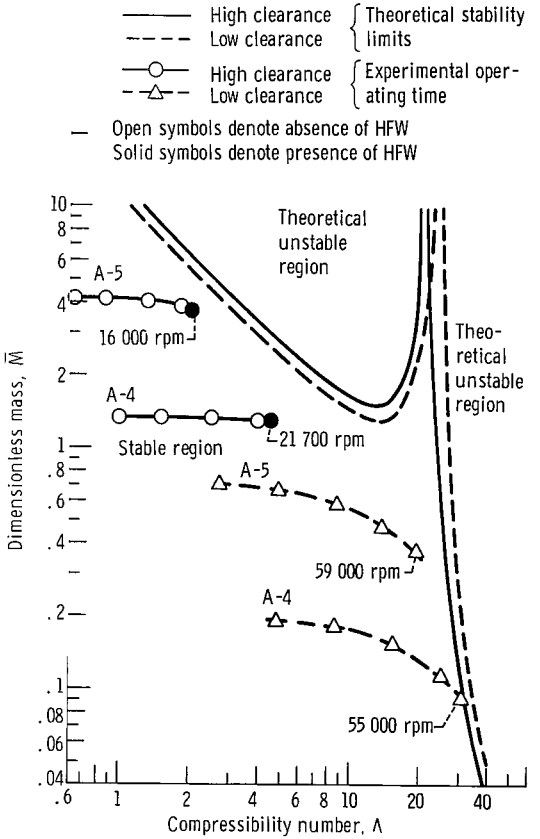

Figure 10. - Comparison of theoretical and experimental stability data for rotors A-4 and A-5.

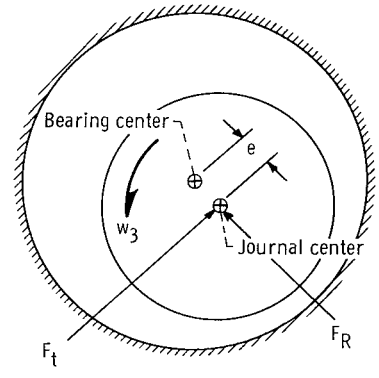

Figure 11. - Steady-state whirling of journal bearing.

NASA-Langley, 1968 —— 15 E-3992

"The aeronautical and space activities of the United States shall be conducted so as to contribute . . . to the expansion of human knowledge of phenomena in the atmosphere and space. The Administration shall provide for the widest practicable and appropriate dissemination of information concerning its activities and the results thereof."

—NATIONAL AERONAUTICS AND SPACE ACT OF 1958

NASA SCIENTIFIC AND TECHNICAL PUBLICATIONS

TECHNICAL REPORTS: Scientific and technical information considered important, complete, and a lasting contribution to existing knowledge.

TECHNICAL NOTES: Information less broad in scope but nevertheless of importance as a contribution to existing knowledge.

TECHNICAL MEMORANDUMS: Information receiving limited distribution because of preliminary data, security classification, or other reasons.

CONTRACTOR REPORTS: Scientific and technical information generated under a NASA contract or grant and considered an important contribution to existing knowledge.

TECHNICAL TRANSLATIONS: Information published in a foreign language considered to merit NASA distribution in English.

SPECIAL PUBLICATIONS: Information derived from or of value to NASA activities. Publications include conference proceedings, monographs, data compilations, handbooks, sourcebooks, and special bibliographies.

TECHNOLOGY UTILIZATION PUBLICATIONS: Information on technology used by NASA that may be of particular interest in commercial and other non-aerospace applications. Publications include Tech Briefs, Technology Utilization Reports and Notes, and Technology Surveys.

Details on the availability of these publications may be obtained from:

SCIENTIFIC AND TECHNICAL INFORMATION DIVISION

NATIONAL AERONAUTICS AND SPACE ADMINISTRATION

Washington, D.C. 20546